Vol. 47, No. 4 (2025) 732-742, DOI: 10.24874/ti.1754.09.24.10

Tribology in Industry

www.tribology.rs

RESEARCH

Study on the Effect of Laser Cleaning Power and Scanning Frequency on Surface Properties and Coating Adhesion of ASTM A36 Steel

Eko Sasmito Hadi[a,*], Ahmad Fidaus[a], Untung Budiarto[a], Muhammad Raaflie Caesar Putra Hadi[a], Rafigo[a], Mohammad Tauviqirrahman[b], J. Jamari[b]

[a]*Department Naval Architecture, Faculty of Engineering, Diponegoro University, Jl. Prof Sudharto, Tembalang, Semarang, Central Java 50275, Indonesia,*
[b]*Laboratory for Engineering Design and Tribology, Faculty of Engineering, Department of Mechanical Engineering, Diponegoro University Indonesia.*

Keywords:

Laser cleaning
Laser parameters
Surface engineering
Coatings
Contact mechanics

* Corresponding author:

Eko Sasmito Hadi
E-mail: ekosasmito@ft.undip.ac.id

Received: 18 September 2025
Revised: 29 October 2025
Accepted: 7 November 2025

A B S T R A C T

Surface conditioning is essential for improving coating adhesion and corrosion resistance in marine infrastructure. While abrasive blasting remains conventional, its environmental and health drawbacks have prompted the development of cleaner surface technologies. This study investigates fiber laser cleaning as a sustainable, high-precision alternative for ASTM A36 steel commonly used in maritime platforms. The experiment explores the influence of laser power (600–1000 W) and scanning frequency (60–100 Hz) on surface morphology and coating adhesion. Results reveal a non-linear correlation between parameters and surface roughness (Ra: 60–98 µm), transitioning from anisotropic, scan-aligned textures at lower power to isotropic microstructures at higher power. Adhesion strength varied between 5.8 and 12.3 MPa, governed more by surface texture complexity than by Ra magnitude alone. The findings establish a process–structure–property linkage, demonstrating how laser-induced topographies enhance mechanical interlocking and interfacial energy compatibility key factors for coating durability. Ultimately, this study positions laser cleaning as an efficient, scalable surface modification method. It bridges the gap between fundamental material understanding and industrial application, providing a technical basis for optimizing laser parameters toward predictive modelling, energy-efficient maintenance, and advanced corrosion mitigation in marine surface engineering.

1. INTRODUCTION

The maritime industry continues to face persistent challenges in corrosion control, requiring solutions that balance structural durability with environmentally responsible surface preparation. Abrasive blasting, although widely implemented [1,2], is limited by process variability driven by the type, size, and operational parameters of the grit, and by the generation of hazardous particulate waste [3,4]. Efforts to incorporate ecofriendly abrasives and optimise blasting parameters have produced partial improvements [5-10], but these measures are insufficient to address the full scope of environmental and regulatory demands.

Recent advances in surface engineering have shifted the focus toward controlled modification of surface energy to improve coating adhesion and long-term protection. Methods such as laser surface texture [11], atmospheric-pressure plasma treatments [12], and hybrid approaches allow for precise surface functionalization. Research has established that initial adhesion is predominantly influenced by surface roughness, while long-term durability depends on surface chemistry and wettability [13-15]. Even with improvements in epoxy-based and fouling-release coatings, performance remains highly sensitive to substrate preparation quality [2,11,16].

Laser cleaning (LC) has emerged as a promising alternative, offering superior precision, reduced waste, and minimal substrate damage compared to traditional mechanical methods [1]. Using thermal ablation, photomechanical stress, and plasma-induced removal, LC effectively removes oxide layers and coatings from various metals [17-19]. Empirical evidence indicates that LC can achieve ISO 8501-1 Sa 2.5 cleanliness with sub-kilowatt energy inputs, while significantly reducing emissions and post-process contamination [1,2].

Despite the proven efficacy in multiple materials, including aluminium alloys and carbon steels, studies on ASTM A36, an essential material in maritime structures, remain limited. Previous work [11] shows that nanosecond laser structuring enhances coating adhesion and corrosion resistance on A36 steel, yet often isolates single performance parameters and lacks methodological alignment with standards such as ISO 8501-1, ASTM D4417, D4414, and D4541.

Moreover, the combined influence of laser power and scanning frequency on surface morphology and adhesion for A36 steel is underexplored. Findings from studies on other substrates indicate that excessive energy densities can induce oxidation, microstructural instability, and thermal damage [12], underscoring the importance of optimizing operational parameters.

Comprehensive evaluations of how laser power and scanning frequency jointly affect roughness, surface topography, and coating adhesion on ASTM A36 steel are absent under industry standard protocols. Addressing this gap is crucial for scaling LC from laboratory research to shipyard operations.

This work investigates ASTM A36 steel treated with fiber laser systems operating at 600–1000 W and 60 to 100 Hz. It examines the interaction of these parameters with the roughness (Ra), three-dimensional morphology, and pull-off adhesion strength, all assessed by standards ISO 8501-1, ASTM D4417, D4414, and D4541.

The findings provide quantitative guidelines for the selection of LC parameters, highlighting its potential to replace abrasive blasting in corrosion-critical marine applications. The results also establish a foundation for predictive modelling and life-cycle assessment of LC-based coating systems.

2. MATERIAL AND METHOD

2.1 Material specification

Specimens measuring 50 × 50 × 6 mm were machined from ASTM A36 structural steel plates, acquired from Baowu International Trade (Shandong) Co., Ltd. [20]. The choice of ASTM A36 reflects its prevalence in maritime structural applications due to its robust mechanical properties, weldability, and performance in corrosive environments [11]. The composition of the material, according to the SS400 / JIS G3101 classification, is summarized in Table 1.

Table 1. Chemical composition of ASTM A36 steel [21].

Element	Elements – Al composition/wt.%				
	Fe	C	Mn	P	S
Standard	-	-	-	≤0.05	≤0.05
Test	99.5	0.0066	0.206	0.003	0.003

2.2 Coating system

The top coat used in this study was Futura Classic, a polyurethane-based system manufactured by JOTUN [22]. Renowned for its high durability, chemical resistance, and gloss retention, Futura Classic is widely deployed in marine infrastructure, especially for superstructures, decks, and upper surfaces exposed to UV radiation and mechanical wear. Its application in this experiment was selected to emulate operational marine conditions and evaluate coating–substrate interactions after laser cleaning.

The curing time of Futura Classic polyurethane topcoat is determined strictly by time and temperature conditions according to manufacturer specifications (JOTUN) and does not depend on substrate surface roughness. All samples were cured under identical conditions (24 hours at 25°C, 50% RH) to ensure that adhesion test results exclusively reflected surface preparation effects. Surface roughness may affect adhesion strength after curing, but not the required curing duration itself.

2.3 Laser cleaning setup

A fiber-coupled Nd:YAG laser system (LW1500, Daiden) with a nominal power output of 1500 W and a wavelength of 1080 ± 10 nm was used for surface preparation [23]. Process variables included five discrete peak power settings and five scanning frequencies, outlined in Table 2.

Table 2. Laser cleaning parameters.

Item	Value
Scanning Frequency	60 Hz, 70 Hz, 80 Hz, 90 Hz, 100 Hz
Scan width	30.0 mm
Peak power	600, 700, 800, 900, 1000 Watt
Duty cycle	100%
Frequency	20 kHz

These parameters were selected based on operational feasibility and prior empirical evidence supporting their influence on surface morphology and oxide removal efficacy [24,25]. The scan speed was calculated using the formula: scan speed (mm/s) = scan width (mm) × scanning frequency (Hz). With a fixed scan width of 30.0 mm, the scan speed ranged from 1800 mm/s (at 60 Hz) to 3000 mm/s (at 100 Hz).

2.4 Experimental procedure overview

The experimental protocol is illustrated schematically in Fig. 1. After preparing the steel substrates, laser ablation was performed using the defined power–frequency matrix. Surface roughness data were acquired to evaluate morphological changes after cleaning. Subsequently, Futura Classic was applied under controlled conditions. Wet and dry film thicknesses were recorded. Final performance assessment was conducted through pull-off adhesion testing to determine the interfacial strength.

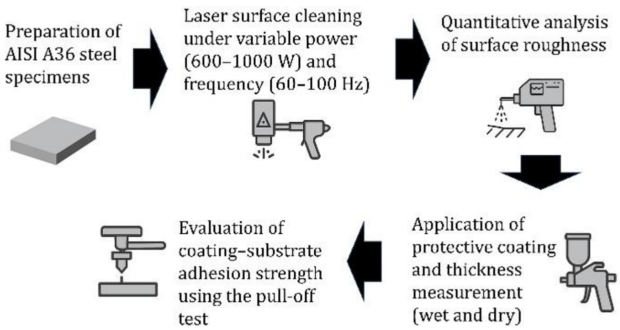

Fig. 1. Schematic overview of experimental workflow including laser treatment, coating application, and post-processing evaluation.

2.5 Visual surface characterization

Surface cleanliness was evaluated according to ISO 8501-1 standards [26], using comparative visual inspection under 50× magnification with a 34 MP trinocular metallographic microscope. Treated surfaces were evaluated against the Sa 3 reference standard, allowing for a qualitative assessment of the efficiency of contaminant removal. The image sets are shown in Fig. 2 and Fig. 3.

(a) (b) (c)

Fig. 2. Visual comparison of substrate surfaces before and after laser cleaning alongside ISO Sa 3 reference: (a) before laser cleaning, (b) after laser cleaning, and (c) SA-3 ISO8501-1 standard.

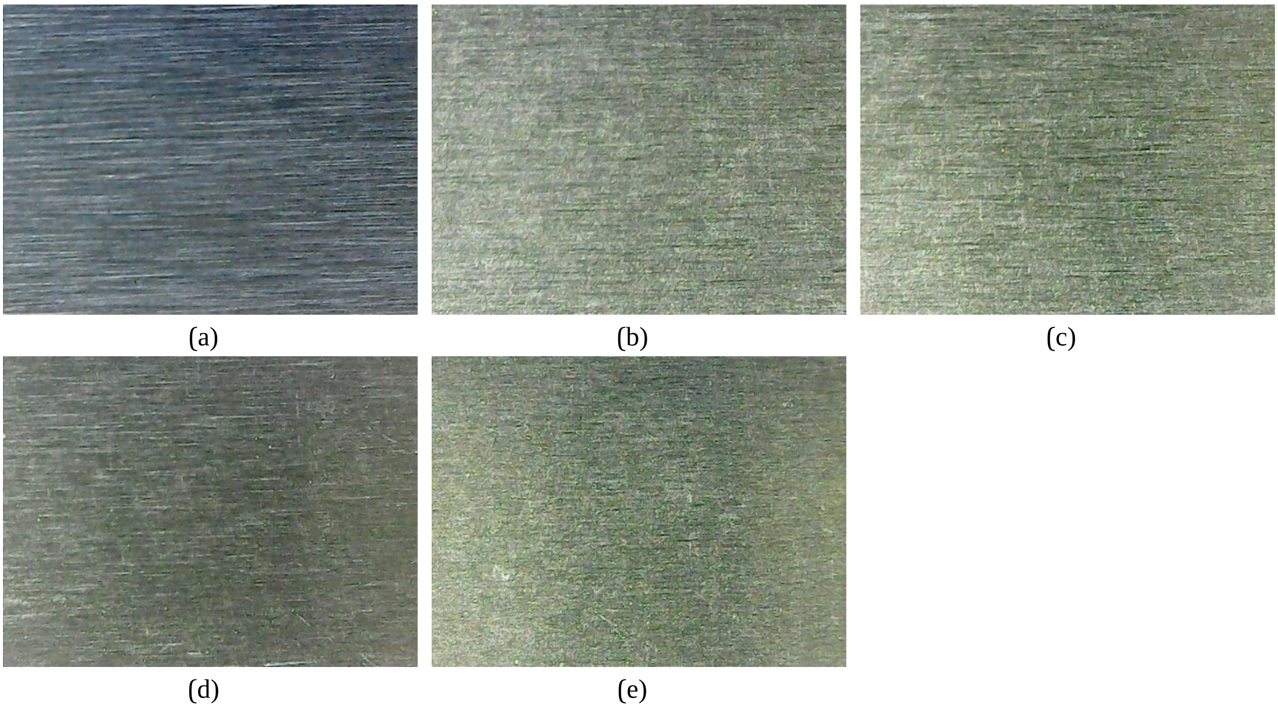

Fig. 3. Microscopic imagery of laser-treated substrates at varying power levels (60 Hz fixed frequency), at laser parameters of (a) 600Watt power, (b) 700Watt, (c) 800Watt, (d) 900 Watt and (e) 1000 Watt.

2.6 Quantitative surface roughness measurement

The surface roughness (Ra) was performed using a contact-type profilometer (Elcometer-224), according to ASTM D4417 [27]. Each specimen was subjected to twenty consecutive measurements to ensure statistical reliability, consistent with the standards for field repeatability [28,29]. A representative profilogram for 600 W/60 Hz is shown on Fig. 4, while a comparative summary of all conditions is illustrated in Fig. 8.

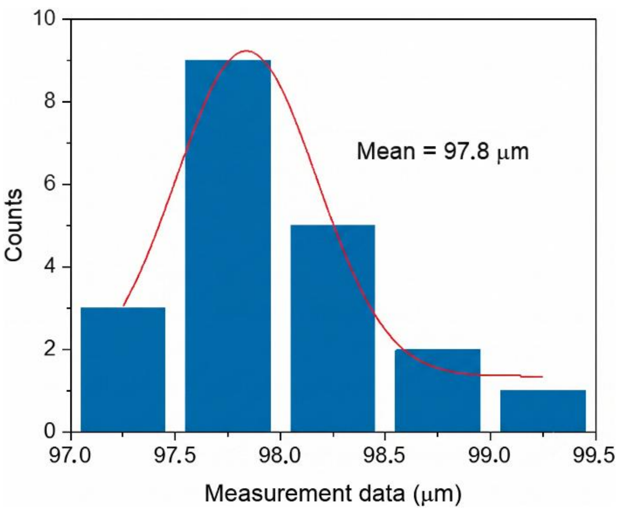

Fig. 4. Surface roughness profile under 600 W and 60 Hz parameter set.

2.7 Coating Thickness Evaluation

The wet film thickness (WFT) was measured using notch gauges by ASTM D4414 [30], while the dry film thickness (DFT) was obtained by ultrasonic measurement (UT343D). The coating application was standardized to 500 μm WFT across all samples to isolate the impact of laser-cleaned substrates on film formation. Fig. 5, presents dry coating thickness at 60 Hz across power levels of 600–1000 W, with labelled data points. Fig. 6, compares wet and dry coating thicknesses across scanning frequencies of 60–100 Hz, with annotations for each parameter.

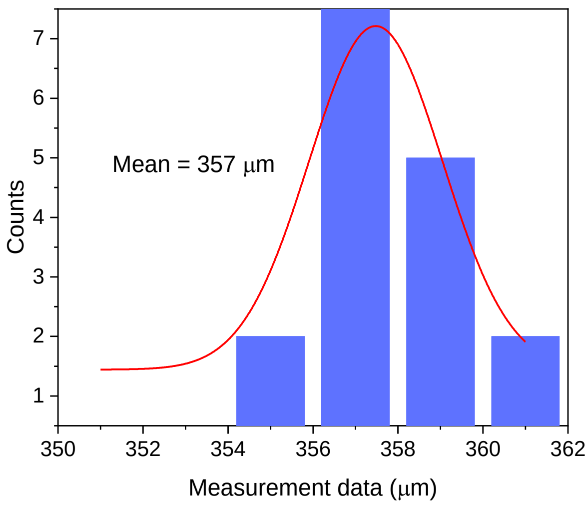

Fig. 5. Dry film thickness at 60 Hz frequency.

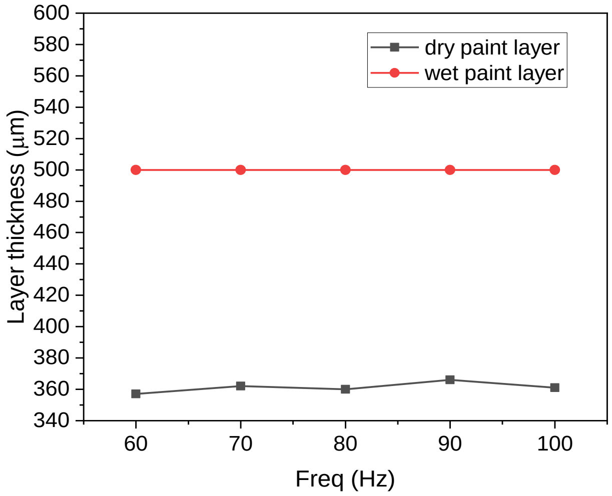

Fig. 6. WFT and DFT comparison across multiple scanning frequencies.

2.8 Adhesion strength evaluation

The adhesion strength was evaluated using the pull-off test method according to ASTM D4541 [31], using a portable hydraulic adhesion tester. Each condition was tested using 20 replicates, allowing the evaluation of the mean adhesion strength and its variation. The critical threshold for industrial acceptance was established at 5 MPa, as specified in NORSOK M-501. The results of a representative test under 600 W and 60 Hz are shown on Fig. 7, with broader trends consolidated in Fig. 10.

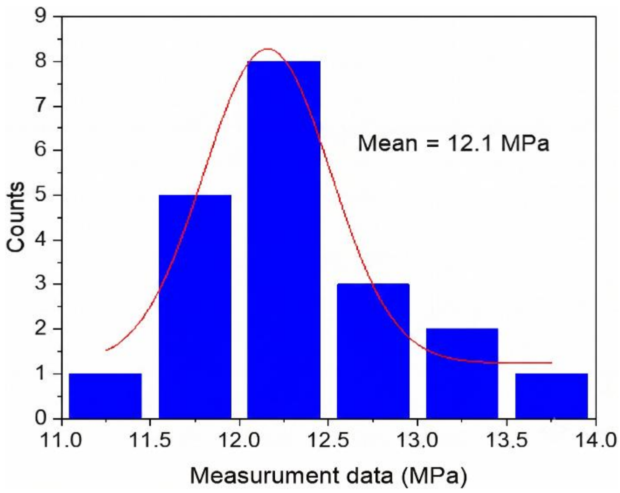

Fig. 7. Representative pull-off adhesion results at 600 W and 60 Hz.

3. RESULTS AND ANALYSIS

3.1 Power and frequency

The interplay between scanning frequency and laser power profoundly influences the roughness (Ra) of laser-cleaned substrates, as demonstrated in Fig. 8. Within the 60–80 Hz range, most laser power settings produce a consistent reduction in Ra values with increasing frequency. This trend is attributable to the shorter dwell time of the laser beam at higher frequencies, which limits the heat accumulation and attenuates excessive surface melting. The observed reduction in Ra under these conditions is consistent with established principles of laser-material interaction documented in prior empirical and computational studies [32-36].

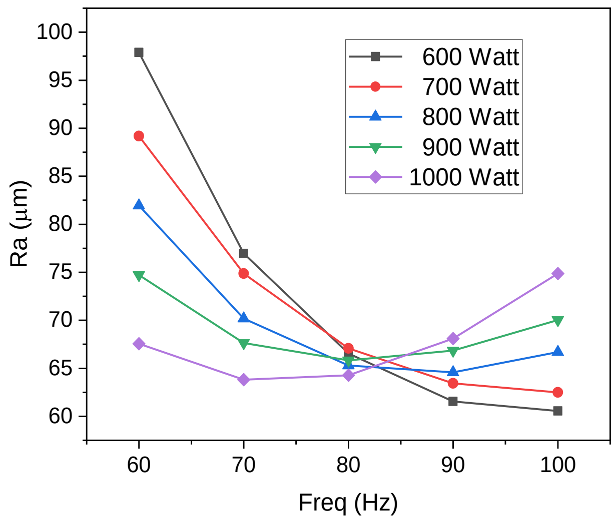

Fig. 8. Variation in surface roughness (Ra) as a function of scanning frequency and laser power.

As the scanning frequency increases, the energy delivered per unit area decreases, promoting milder surface treatment. This minimizes subsurface thermal gradients and facilitates smoother morphologies because of reduced ablation depth. The literature supports this inverse relationship between scan frequency and roughness, particularly in low to mid-power regimes [37,38].

However, this trend becomes non-linear at higher power inputs (800 to 1000 W). In the frequency domain beyond 80 Hz, the Ra values exhibit an inflection, surprisingly increasing rather than decreasing. This phenomenon can be attributed to excessive localized heating, despite the reduced interaction time. The high energy density initiates deeper ablation and destabilizes melt pool dynamics, producing microstructural irregularities such as elevated peak–valley topographies. These results are consistent with the findings of researchers investigating laser-induced thermophysical phenomena at elevated fluence levels [39-42].

The comprehensive data set demonstrates that Ra values range from 60 to 98 µm, highlighting the sensitivity of surface morphology to parameter selection. While elevated roughness can enhance coating adhesion via mechanical anchoring, this benefit is context-specific and depends on the adhesive's rheological properties and the coating-substrate interaction mechanism. Consequently, the optimal operational window appears to lie within the 60–70 Hz frequency band, particularly for applications that prioritise surface texture without compromising thermal integrity [43].

3.2 Surface roughness and adhesion of coating layers

The surface morphology resulting from laser cleaning, as visualized in Fig. 9, exhibits a clear dependence on laser power under a constant scanning frequency of 60 Hz. At 600 W (Fig. 9a), the surface shows pronounced linear patterns aligned with the laser scanning trajectory. These structures are characterized by well-defined ridges and troughs, resulting from localized melting and re-solidification driven by spatially controlled thermal gradients. Significant peak-to-valley variations correlate with elevated surface roughness (Ra ~98 µm), indicating extensive surface modulation following moderate thermal input.

The underlying mechanisms involve rapid heat absorption that exceeds the melting threshold, initiating transient liquefaction of the steel substrate. The molten material, influenced by laser-induced recoil pressure and surface tension gradients (i.e., Marangoni effect), undergoes convective flow and resolves into directional waveforms. The cross-sectional image in Fig. 9b confirms the presence of different morphological features, indicative of a melt-driven ablation regime where the topography promotes increased interfacial area and potential anchorage for coating applications.

In contrast, the surface loses its anisotropic character at 1000 W power input Fig. 9c and evolves into a more chaotic isotropic profile. This reflects a regime dominated by excessive energy flux, where deeper ablation and turbulent melt dynamics suppress directional structuring. High thermal load generates widespread liquefaction, and subsequent rapid cooling leads to irregular solidification patterns with varying height distributions. These effects are substantiated in Fig. 9d, which shows diminished sharpness in features but enhanced surface complexity, a hallmark of increased energy density processing regimes. Such observations align with recent computational fluid dynamics models and experimental data on high-power laser ablation [44].

These morphological transitions directly influence the adhesion performance, as shown in Fig. 10. At lower laser powers (600–700 W), an increase in the scanning frequency leads to a notable decrease in adhesion strength, from 12.3 MPa at 60 Hz to 5.8 MPa at 100 Hz. This trend correlates with smoother surfaces that reduce the potential for mechanical interlocking and interfacial bonding. However, at higher power levels (particularly 1000 W), the opposite trend is observed: adhesion strength increases progressively with frequency, reaching up to 8.7 MPa. This improvement can be attributed to more favorable micro topographies formed under high-energy densities, even as Ra values decrease.

The complex interplay between surface roughness, topographic heterogeneity, and coating adhesion suggests that Ra alone cannot predict bonding efficacy. Texture anisotropy, peak distribution, and sub-micrometer-scale morphology significantly modulate adhesive behavior [43]. Previous research also indicates that surfaces with moderate roughness and multidirectional micro-characteristics improve wettability and mechanical anchoring [45,46]. Furthermore, engineered micro textures with optimal aspect ratios promote efficient infiltration of coating materials into surface asperities, thus increasing adhesion strength [47,48].

These findings emphasis the need to precisely calibrating laser parameters, particularly power and scanning frequency—to engineer surface morphologies tailored for optimal coating performance. The empirical correlation between process conditions and adhesion metrics underscores the relevance of a parameter-specific approach to laser cleaning. Furthermore, alignment with theoretical and simulation-based predictions reinforces the mechanistic validity of the observed phenomena [44,49].

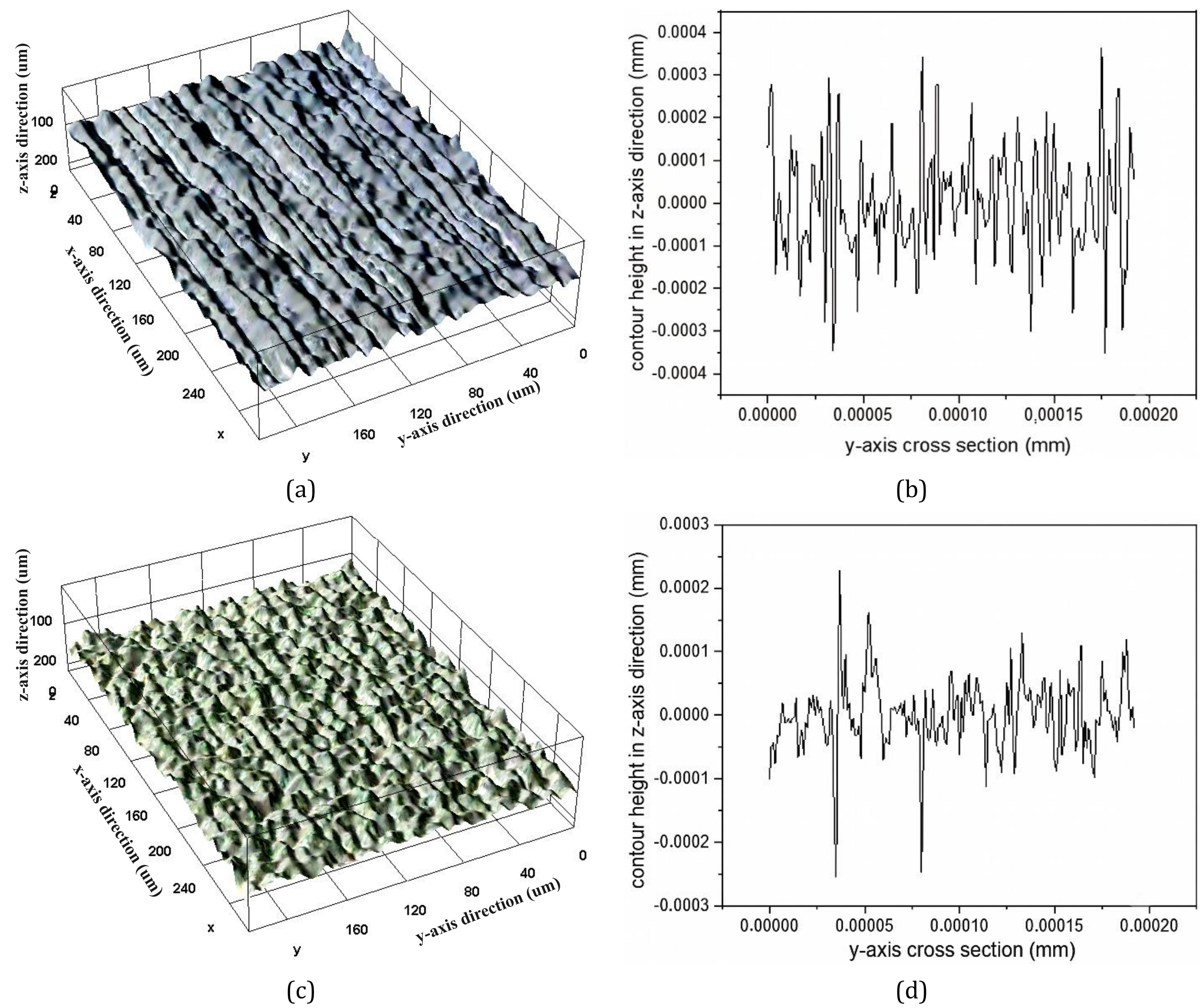

Fig. 9. Surface characterization of laser-treated specimens at 60 Hz frequency across different power levels: (a) topographical profile at 600 W laser power, (b) cross-sectional analysis at 600 W laser power, (c) topographical profile at 1000 W laser power, and (d) cross-sectional analysis at 1000 W laser power.

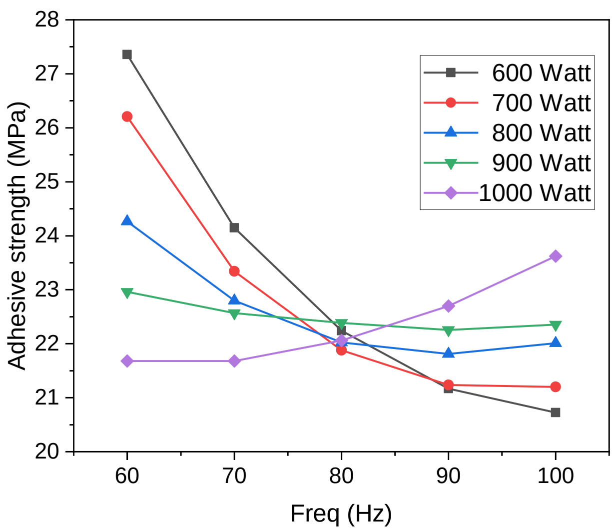

Fig. 10. Adhesion strength of coatings as a function of laser power and scanning frequency.

3.3 Correlation between surface topography and coating performance

Although Sections 3.1 and 3.2 have independently explored the influence of laser process parameters on surface roughness and coating adhesion, a comprehensive interpretation is required to elucidate the mechanistic links between microstructural modifications and their functional implications. This subsection establishes an integrative framework grounded in the process-structure-property relationships critical in advanced surface engineering.

The morphological variations captured in Fig. 9 reveal two different regimes of topographic evolution. At a lower laser power of 600 W, the substrate develops ordered, anisotropic patterns driven by spatially controlled thermal gradients and directional melt dynamics. In contrast, at 1000 W, a transition occurs toward a more stochastic, isotropic topography resulting from intensified energy input and chaotic melt-pool behaviour. These structural distinctions directly affect the adhesion performance, as illustrated in Fig. 10, where surfaces treated under high-power and high-frequency settings exhibit superior bonding despite lower Ra values.

The underlying adhesion enhancement is attributed to the increased penetration of the coating into multiscale surface asperities, supported by mechanical interlocking and capillarity. This interpretation is consistent with theoretical models in contact mechanics and surface adhesion science, which posit that anisotropic geometry and multidirectional roughness enhance interfacial energy dissipation and bond formation [46,47].

Furthermore, the observed transformation from structured to isotropic morphology with rising energy input corroborates thermodynamic simulations by Narayanan et al. (2021), who demonstrated that turbulence in the molten phase promotes nonuniform solidification, yielding beneficial surface complexity [40]. While visually less uniform, these stochastic morphologies establish multidirectional mechanical anchors that improve coating durability.

A comparative evaluation of Fig. 8, Fig. 9, and Fig. 10 highlights the limitations of using Ra as the sole indicator of coating performance. For example, equivalent Ra values observed at 800 W/60 Hz and 1000 W/80 Hz yield substantially different adhesion strengths, underscoring the importance of considering topographic architecture, feature distribution, and surface energy gradients.

This analysis reinforces a paradigm shift in laser surface engineering, from reliance on scalar metrics like Ra to a multidimensional interpretation incorporating morphological complexity and functional texture. This shift is pivotal for optimizing laser cleaning and informing predictive design frameworks in high-performance coating systems [50].

To support this synthesis, Fig. 8, Fig. 9, and Fig. 10 are revisited as integral visual datasets. Their triangulated analysis provides a robust foundation for interpreting how combinations of laser power and frequency govern microstructural development and how these changes influence the resultant mechanical integrity and longevity of coating–substrate systems.

Prior studies have established a relationship between scan speed and surface morphology during laser cleaning processes. Seo et al. (2022) demonstrated that higher scan speeds resulted in smoother surface topographies during laser cleaning of steel surfaces [33]. Similarly, Xue et al. (2022) reported that increasing scan speeds led to more homogeneous surface structures on carbon steel [51]. While this study focused on the combined effects of laser power and scanning frequency as integrated operational parameters, reflecting typical industrial practice where these variables are optimized together rather than separately, the correlation between Scan Speed and surface morphology is clearly demonstrated in Figure 8 and subsequent analyses. Future studies will incorporate dedicated experimental designs to isolate the individual effects of scan speed on surface topography.

4. CONCLUSION

This study provides a detailed examination of how the cleaning parameters of the laser-namely, the laser power and scanning frequency affect the surface morphology and interfacial coating of ASTM A36 steel. Through a systematic analysis of surface roughness profiles, topographical transitions, and adhesion strength, the research highlights how these variables collectively influence the functional efficacy of laser-prepared surfaces, particularly in corrosive industrial environments.

The principal conclusions derived from the investigation are as follows:

1. Surface roughness (Ra) exhibited a non-linear dependency on laser parameters, ranging from 60 to 98 μm. A reduction in Ra was generally observed with increasing scanning frequency (60–80 Hz) under moderate power conditions, while excessive power input (800-1000 W) at high frequencies (>80 Hz) reversed this trend due to intensified thermal ablation.

2. Different topographical architectures were observed on energy density. Lower power settings generated directional, anisotropic patterns aligned with the scanning path, whereas higher power conditions promoted irregular, isotropic textures resulting from chaotic melt dynamics. These microstructural transitions are directly related to the thermal-fluid behavior of the melt pool and the solidification kinetics.
3. The adhesion strength of the applied coating was sensitive to roughness morphology and combinations of laser setting. While the increased frequency diminished adhesion at low powers, it enhanced it at high powers. This confirms that microstructural complexity and spatial distribution of surface characteristics – rather than average roughness alone –are more reliable predictors of adhesion performance.
4. These findings underscore the importance of adopting multidimensional surface characterization strategies that integrate roughness metrics, textural anisotropy, and morphological mapping. In doing so, laser cleaning has been validated as an environmentally advantageous alternative to abrasive techniques and a precision-engineered process for customizing surface functionality.

This study advances the scientific discourse on laser-based surface engineering in maritime and structural applications by delineating straightforward process–structure–property relationships. The results provide a framework for optimizing laser parameters to enhance coating performance while maintaining energy efficiency. Further research should explore fatigue resistance and long-term environmental exposure of laser-treated substrates, investigate the integration of multilayer coating systems, and develop predictive computational models to support industrial-scale deployment.

Acknowledgement

This research was financially supported by The Faculty of Engineering, Diponegoro University, Indonesia, through Strategic Research Grant 2024, number 204/S/Perkapalan/4/UN7.F3/PP/III/2024.

REFERENCES

[1] A. Kim, S. Kainuma, and M. Yang, "Surface Characteristics and Corrosion Behavior of Carbon Steel Treated by Abrasive Blasting," *Metals*, vol. 11, no. 12, p. 2065, Dec. 2021, doi: 10.3390/met11122065.

[2] I. S. Dos Santos, L. J. De Carvalho, L. Y. Reznik, and S. L. D. C. Brasil, "Anti-corrosive properties of two epoxy primer systems applied to steel surfaces prepared with various mechanical abrasive treatments," *Journal of Adhesion Science and Technology*, vol. 34, no. 22, pp. 2467–2483, Nov. 2020, doi: 10.1080/01694243.2020.1767476.

[3] N. Lashmar et al., "Environmental impacts of abrasive blasting of transmission towers in protected areas," *Journal of Environmental Management*, vol. 252, p. 109430, Dec. 2019, doi: 10.1016/j.jenvman.2019.109430.

[4] H. Zakaria et al., "Dust Exposure Monitoring: Abrasive Blasting Dust from Cleaning Process in Marine Industry," *International Journal of Integrated Engineering*, vol. 11, no. 5, Aug. 2019, doi: 10.30880/ijie.2019.11.05.013.

[5] N. Anaç and Z. Doğan, "Effect of Organic Powders on Surface Quality in Abrasive Blasting Process," *Processes*, vol. 11, no. 7, p. 1925, Jun. 2023, doi: 10.3390/pr11071925.

[6] İ. Kılınç, M. Budakçı, and M. Korkmaz, "The use of environmentally friendly abrasive blasting media for paint removal from wood surfaces," *BioResources*, vol. 18, no. 1, pp. 1185–1205, Dec. 2022, doi: 10.15376/biores.18.1.1185-1205.

[7] V. Alankaya and U. B. Celebi, "Investigation of alternative blasting process in terms of impact behaviour of blasting materials for green shipyards," *International Journal of Global Warming*, vol. 7, no. 4, p. 499, 2015, doi: 10.1504/IJGW.2015.070050.

[8] I. Zulkarnain et al., "Sustainability-Based Characteristics of Abrasives in Blasting Industry," *Sustainability*, vol. 13, no. 15, p. 8130, Jul. 2021, doi: 10.3390/su13158130.

[9] W. Czepułkowska-Pawlak, E. Wołowiec-Korecka, and L. Klimek, "The Surface Condition of Ni-Cr after SiC Abrasive Blasting for Applications in Ceramic Restorations," *Materials*, vol. 13, no. 24, p. 5824, Dec. 2020, doi: 10.3390/ma13245824.

[10] W. Czepułkowska, E. Wołowiec-Korecka, and L. Klimek, "The Condition of Ni-Cr Alloy Surface After Abrasive Blasting with Various Parameters," *Journal of Materials Engineering and Performance*, vol. 29, no. 3, pp. 1439–1444, Mar. 2020, doi: 10.1007/s11665-019-04399-z.

[11] S. J. Caraguay, T. S. Pereira, R. O. Giacomelli, A. Cunha, M. Pereira, and F. A. Xavier, "The effect of laser surface textures on the corrosion resistance of epoxy coated steel exposed to aggressive environments for offshore applications," *Surface and Coatings Technology*, vol. 437, p. 128371, May 2022, doi: 10.1016/j.surfcoat.2022.128371.

[12] A. Maroofi, N. Navab Safa, and H. Ghomi, "Atmospheric air plasma jet for improvement of paint adhesion to aluminium surface in industrial applications," *International Journal of Adhesion and Adhesives*, vol. 98, p. 102554, Apr. 2020, doi: 10.1016/j.ijadhadh.2020.102554.

[13] J. P. B. Van Dam, S. T. Abrahami, A. Yilmaz, Y. Gonzalez-Garcia, H. Terryn, and J. M. C. Mol, "Effect of surface roughness and chemistry on the adhesion and durability of a steel-epoxy adhesive interface," *International Journal of Adhesion and Adhesives*, vol. 96, p. 102450, Jan. 2020, doi: 10.1016/j.ijadhadh.2019.102450.

[14] S.-H. Eom, S.-S. Kim, and J.-B. Lee, "Assessment of Anti-Corrosion Performances of Coating Systems for Corrosion Prevention of Offshore Wind Power Steel Structures," *Coatings*, vol. 10, no. 10, p. 970, Oct. 2020, doi: 10.3390/coatings 10100970.

[15] S. G. Croll, "Surface roughness profile and its effect on coating adhesion and corrosion protection: A review," *Progress in Organic Coatings*, vol. 148, p. 105847, Nov. 2020, doi: 10.1016/j.porgcoat.2020.105847.

[16] A. Pistone, C. Scolaro, and A. Visco, "Mechanical Properties of Protective Coatings against Marine Fouling: A Review," *Polymers*, vol. 13, no. 2, p. 173, Jan. 2021, doi: 10.3390/polym13020173.

[17] J.-E. Kim and J.-D. Kim, "A study on the removal of paint and oxide layer on the steel surface by laser beam scanning method," *International Journal of Modern Physics B*, vol. 35, no. 14n16, p. 2140006, Jun. 2021, doi: 10.1142/S0217979221400063.

[18] G. Zhu, S. Wang, W. Cheng, Y. Ren, and D. Wen, "Corrosion and wear performance of aircraft skin after laser cleaning," *Optics & Laser Technology*, vol. 132, p. 106475, Dec. 2020, doi: 10.1016/ j.optlastec.2020.106475.

[19] Z. Zhou, W. Sun, J. Wu, H. Chen, F. Zhang, and S. Wang, "The Fundamental Mechanisms of Laser Cleaning Technology and Its Typical Applications in Industry," *Processes*, vol. 11, no. 5, p. 1445, May 2023, doi: 10.3390/pr11051445.

[20] "Carbon Steel Plate-Baowu International Trade (Shandong) Co., Ltd." https://www.cnbwsteel.com/products/carbon_steel/carbon_steel_plate/a36_carbon_steel_plate.html, [accessed Aug. 21, 2024]

[21] R. D. Sulamet-Ariobimo, J. W. Soedarsono, T. Sukarnoto, A. Rustandi, Y. Mujalis, and D. Prayitno, "Tensile properties analysis of AA1100 aluminium and SS400 steel using different JIS tensile standard specimen," *Journal of Applied Research and Technology*, vol. 14, no. 2, pp. 148–153, Apr. 2016, doi: 10.1016/j.jart.2016.03.006.

[22] JOTUN, "Futura Classic - JOTUN." https://www.jotun.com/ww-en/industries /products/Futura-Classic, [accessed Aug. 23, 2024].

[23] Aneka Mega Energi, "Laser Welding Daiden LW 1500 | Aneka Mega Energi," Aneka Mega Energi, Jul. 27, 2024. https://anekamega.com/product/laser-welding-daiden-lw-1500

[24] Y. Lu, L. Yang, M. Wang, and Y. Wang, "Improved thermal stress model and its application in ultraviolet nanosecond laser cleaning of paint," *Applied Optics*, vol. 59, no. 25, p. 7652, Sep. 2020, doi: 10.1364/AO.398101.

[25] X. Li et al., "Influence of ns-Laser Cleaning Parameters on the Removal of the Painted Layer and Selected Properties of the Base Metal," *Materials*, vol. 13, no. 23, p. 5363, Nov. 2020, doi: 10.3390/ma13235363.

[26] *Preparation of steel substrates before application of paints and related products — Visual assessment of surface cleanliness — Part 1: Rust grades and preparation grades of uncoated steel substrates and of steel substrates after overall*, ISO 8501-1:2007, 2007.

[27] *D4417 Standard Test Methods for Field Measurement of Surface Profile of Blast Cleaned Steel*, ASTM D4417.

[28] F. Habibzadeh, "Data Distribution: Normal or Abnormal?," *Journal of Korean Medical Science*, vol. 39, no. 3, p. e35, 2024, doi: 10.3346/jkms.2024.39.e35.

[29] P. Mishra, C. Pandey, U. Singh, A. Gupta, C. Sahu, and A. Keshri, "Descriptive statistics and normality tests for statistical data," *Ann Card Anaesth*, vol. 22, no. 1, p. 67, 2019, doi: 10.4103/aca.ACA_157_18.

[30] *D4414 Standard Practice for Measurement of Wet Film Thickness by Notch Gages*, ASTM D4414, 2020.

[31] *D4541 Standard Test Method for Pull-Off Strength of Coatings Using Portable Adhesion Testers*, ASTM D4541.

[32] M. F. Erinosho, E. T. Akinlabi, and O. T. Johnson, "Effect of Scanning Speed on the Surface Roughness of Laser Metal Deposited Copper on Titanium Alloy," *Materials Research*, vol. 22, no. 5, p. e20190297, 2019, doi: 10.1590/1980-5373-mr-2019-0297.

[33] Y. Seo, S. Son, and D. Lee, "A study of laser cleaning to remove by-products occurring after arc welding," *Materials Chemistry and Physics*, vol. 288, p. 126375, Sep. 2022, doi: 10.1016/j.matchemphys.2022.126375.

[34] T. T. Vu and H. H. Hoang, "Investigating the Effect of Pulsed Fiber Laser Parameters on the Roughness of Aluminium Alloy and Steel Surfaces in Cleaning Processes," *Lasers Manuf. Mater. Process.*, vol. 8, no. 2, pp. 113–124, Jun. 2021, doi: 10.1007/s40516-021-00139-1.

[35] P. Jaritngam, V. Saetang, and C. Dumkum, "Laser Surface Polishing of Ti6Al4V Titanium Alloy in Air, Nitrogen and Argon Environments," *Key Engineering Materials*, vol. 897, pp. 15–20, Aug. 2021, doi: 10.4028/www.scientific.net/KEM.897.15.

[36] A. Gisario, M. Barletta, and F. Veniali, "Laser polishing: a review of a constantly growing technology in the surface finishing of components made by additive manufacturing," *The International Journal of Advanced Manufacturing Technology*, vol. 120, no. 3–4, pp. 1433–1472, May 2022, doi: 10.1007/s00170-022-08840-x.

[37] M. Madić, P. Janković, M. Radovanović, and D. Petković, "Analysis and optimization of surface roughness in co2 laser cutting of p265gh steel," *Proceedings on Engineering Sciences*, vol. 1, no. 1, pp. 436–439, May 2019, doi: 10.24874/PES01.01.057.

[38] L. Gurau and A. Petru, "The Influence of CO2 Laser Beam Power Output and Scanning Speed on Surface Quality of Norway Maple (Acer platanoides)," *BioResources*, vol. 13, no. 4, pp. 8168–8183, Sep. 2018, doi: 10.15376/biores.13.4.8168-8183.

[39] C. A. Biffi et al., "Ultrashort Laser Texturing of Superelastic NiTi: Effect of Laser Power and Scanning Speed on Surface Morphology, Composition and Wettability," *Metals*, vol. 13, no. 2, p. 381, Feb. 2023, doi: 10.3390/met13020381.

[40] V. Narayanan, R. Singh, and D. Marla, "A computational model to predict surface roughness in laser surface processing of mild steel using nanosecond pulses," *Journal of Manufacturing Processes*, vol. 68, pp. 1880–1889, Aug. 2021, doi: 10.1016/j.jmapro. 2021.07.016.

[41] M. Ma et al., "Investigation of the Surface Integrity of Q345 Steel After Nd:YAG Laser Cleaning of Oxidized Mining Parts," *Coatings*, vol. 10, no. 8, p. 716, Jul. 2020, doi: 10.3390/coatings10080716.

[42] Z. Wan et al., "Effect of laser power on cleaning mechanism and surface properties," *Applied Optics*, vol. 59, no. 30, p. 9482, Oct. 2020, doi: 10.1364/ AO.399691.

[43] R. Wang, L. Zhan, and Z. Xu, "Characteristic and mechanism of pollution by laser cleaning high-value vehicle parts with a complex structure in remanufacturing industry," *Fundamental Research*, p. S2667325824001419, Apr. 2024, doi: 10.1016/j.fmre.2024.04.002.

[44] J.-E. Kim, J.-M. Lee, J.-H. Hyun, J.-H. Jeong, and J.-D. Kim, "A Study on the Laser Removal of Epoxy Coatings on SS400 Surface by Beam Scanning Patterns," *Coatings*, vol. 11, no. 12, p. 1510, Dec. 2021, doi: 10.3390/coatings11121510.

[45] S. Rajupet, M. Sow, and D. J. Lacks, "Particle adhesion to rough surfaces," *Physical Review E*, vol. 102, no. 1, p. 12904, Jul. 2020, doi: 10.1103/ PhysRevE.102.012904.

[46] D. E. Packham, "Surface energy, surface topography and adhesion," *International Journal of Adhesion and Adhesives*, vol. 23, no. 6, pp. 437–448, Jan. 2003, doi: 10.1016/S0143-7496 (03)00068-X.

[47] S. Su, C. Wang, G. Mi, L. Xiong, W. Zhang, and J. Wang, "A study of the effect of laser micro-texture on bond strength and fracture mechanism of paint layer," *Materials Chemistry and Physics*, vol. 309, p. 128411, Nov. 2023, doi: 10.1016/j.matchemphys.2023.128411.

[48] A. Rudawska, I. Miturska-Barańska, E. Doluk, and E. Olewnik-Kruszkowska, "Assessment of Surface Treatment Degree of Steel Sheets in the Bonding Process," *Materials*, vol. 15, no. 15, p. 5158, Jul. 2022, doi: 10.3390/ma15155158.

[49] Z. Zhang et al., "Surface cleaning of hot-rolled sheet steel by laser ablation of oxide layer using a 100-ns high-repetition frequency pulsed laser," *Optical Engineering*, vol. 56, no. 11, p. 1, Nov. 2017, doi: 10.1117/1.OE.56.11.116114.

[50] G. Zhu et al., "Mechanism and application of laser cleaning: A review," *Optics and Lasers in Engineering*, vol. 157, p. 107130, Oct. 2022, doi: 10.1016/j.optlaseng.2022.107130.

[51] Xue Yafei et al, "Effect of laser scanning speed of the removal quality of rust layer on carbon steel surface.," *Infrared and Laser Engineering*, vol. 51, no. 5, p. 20210389, Jan. 2022, doi: 10.3788/IRLA 20210389.